CONSTRUCTION OF A FAST-SCANNING FAR-INFRARED FABRY-PEROT INTERFEROMETER

by

DAVID SERKES KOMM

B.S., California Institute of Technology (1969)

Submitted in Partial Fulfillment of
the Requirements for the Degree of
Master of Science
at the
MASSACHUSETTS INSTITUTE OF TECHNOLOGY
June, 1973

Signature redacted

Signature of Author_____
Department of Nuclear Engineering
May 11, 1973

Signature redacted

Certified by_____
Thesis Supervisor

Accepted by_____
Chairman, Departmental Committee
on Graduate Students

CONSTRUCTION OF A FAST-SCANNING FAR-INFRARED FABRY-PEROT INTERFEROMETER

by
David Serkes Komm

Submitted to the Department of Nuclear Engineering on May 11, 1973, in partial fulfillment of the requirements for the degree of Master of Science.

A scanning Fabry-Perot interferometer with a free spectral range scan time of less than three milliseconds has been developed for use in the far infrared, $\lambda = 200\mu$ to $\lambda = 1000\mu$. Mirrors were fabricated from metallic mesh. Using mesh of 250 lines/inch, an experimentally determined finesse of $9.3 \pm .3$ was obtained at $\lambda = 337\mu$. With the selection of appropriate mesh, the interferometer should be usable from $\lambda \lesssim 100\mu$ to $\lambda \gtrsim 2$ mm.

Thesis Supervisor: R. A. Blanken
Title: Associate Professor of Nuclear Engineering

ACKNOWLEDGEMENT

The author would like to express his gratitude to Professor R.A. Blanken for his guidance and encouragement during the course of this thesis. Thanks are also due to R.L. McCrory, Jr. for his excellent help in developing the computer codes used in this thesis.

TABLE OF CONTENTS

TABLE OF FIGURES

INTRODUCTION

The purpose of this S.M. thesis is to build a fast-scanning Fabry-Perot interferometer for use in the far-infrared--- microwave region of the spectrum. In this region, electron synchrotron radiation occurs in plasma devices with high magnetic fields. Of particular interest here at MIT, is the synchrotron radiation from the pulsed device, Alcator, upon which the interferometer will be used.

The frequency range that the interferometer must work at is that of the synchrotron radiation fundamental and its first few harmonics, the frequencies being determined by the magnetic field strength. The fundamental is given by qB/m_e which for Alcator, with B = 10 Tesla, gives $qB/m_e = 1.76 \times 10^{12}$ corresponding to a wavelength of 1.07 mm. The synchrotron emission is not a line spectra, however, but rather it is peaked about the fundamental and its harmonics. The interferometer must be capable of operation with wavelengths from 2 mm down to 250μ in order to provide the necessary coverage.

It would be extremely desirable to scan the synchrotron radiation spectrum many times during one pulse of Alcator to obtain a time history of the radiation. Since Alcator is pulsed on for 30 msec. at a time, an interferometer with a scanning repetition rate of 300 cycles/sec. would provide ten complete scans during one pulse.

This then is the thesis: the construction of a scanning Fabry-Perot interferometer capable of operation in the range of .2 mm to 2 mm, a scanning rate of 300 cycles/sec., and as high a finesse as possible.

CHAPTER 1

THEORY OF THE FABRY-PEROT INTERFEROMETER

SEC. 1.1. Introduction to the Fabry-Perot

The Fabry-Perot interferometer makes use of the multiple reflections between two plane parallel surfaces. Consider the arrangement of Fig. 1.1.1 where the two surfaces are very thin compared to the wavelength or incident radiation. Let each surface be described by its complex coefficients of reflection and transmission for amplitudes which are denoted by r and t for radiation incident from outside the separating medium and R and T for radiation incident from inside the medium. The difference in phase between successive beams leaving on the right is:

$$\alpha = 2N \vec{k} \cdot \vec{d} \tag{1.1.1}$$

where $\vec{k}$ is the wave number vector and $\vec{d}$ is the spacing vector. Then the amplitude of each transmitted wave is as indicated in Fig. 1.1.1.

The total transmitted amplitude for m beams is:

$$t_m = t_1 T_2 e^{i\alpha/2} + t_1 T_2 R_1 R_2 e^{i3\alpha/2} + t_1 T_2 R_1^2 R_2^2 e^{i5\alpha/2} + \ldots + t_1 T_2 R_1^{m-1} R_2^{m-1} e^{i(2m-1)\alpha/2} \tag{1.1.2}$$

Summing the geometric series gives:

$$t_m = t_1 T_2 e^{i\alpha/2} (1 - R_1^m R_2^m e^{im\alpha}) / (1 - R_1 R_2 e^{i\alpha}) \tag{1.1.3}$$

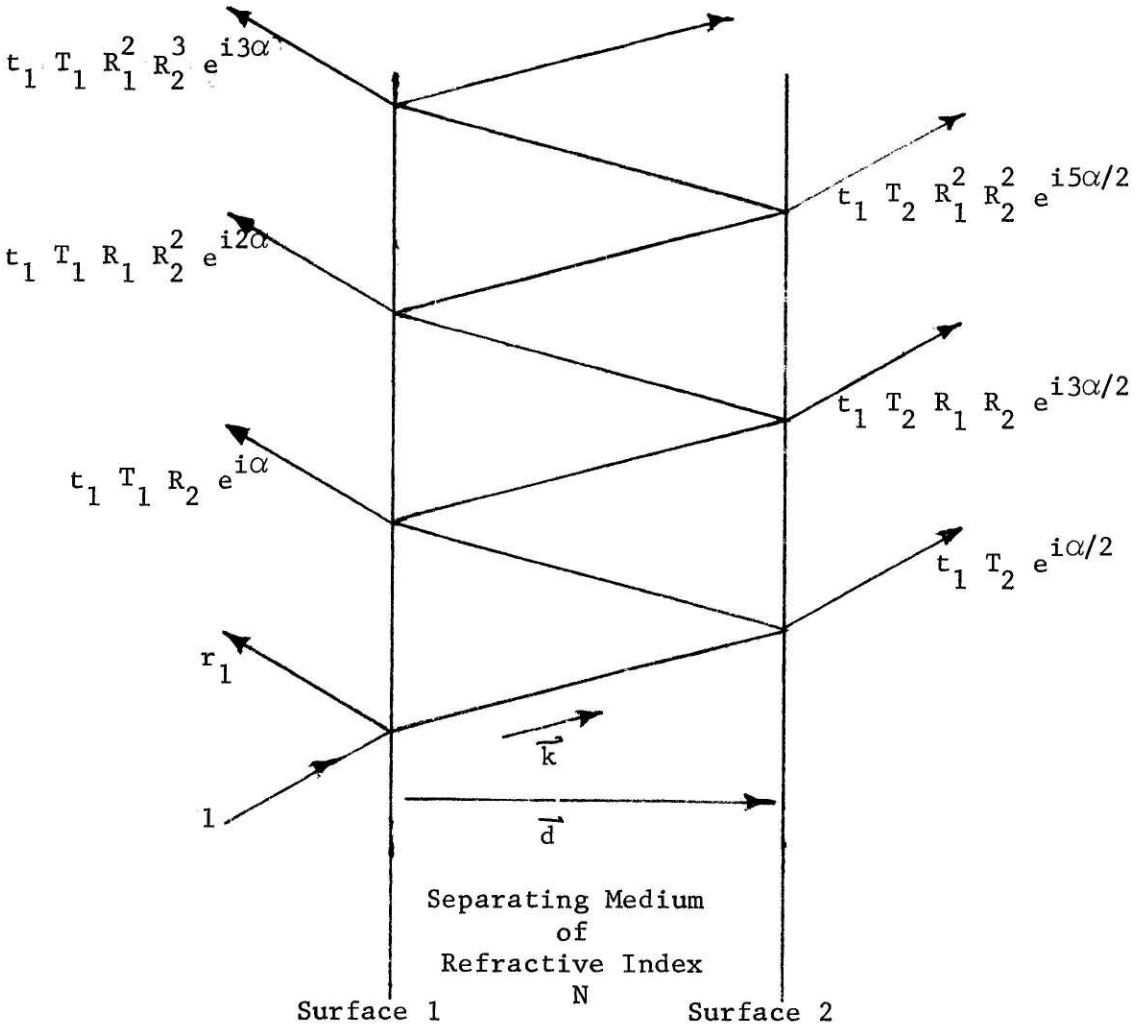

Fig. 1.1.1

Multiple Reflections in a Fabry-Perot Interferometer

(After Steel)[1]

for $m \to \infty$

$$(1.1.4) \qquad t = \frac{t_1 T_2 \, e^{i\alpha/2}}{1 - R_1 R_2 \, e^{i\alpha}} = \frac{\mathfrak{C} \, e^{i\zeta}}{1 - \rho \, e^{i\epsilon}}$$

where

$$(1.1.5) \qquad \mathfrak{C} = | t_1 T_2 | \qquad \rho = | R_1 R_2 |$$

$$\zeta = \alpha/2 + \arg t_1 + \arg t_2 \qquad \epsilon = \alpha + 2\varphi$$

$$\varphi = \frac{\arg R_1 + \arg R_2}{2}$$

The transmitted intensity is the Airy formula

$$(1.1.6) \qquad \tau(\epsilon) = t \, t^* = \frac{\mathfrak{C}^2}{1 - 2\rho \cos\epsilon + \rho^2}$$

For a Fabry-Perot with air as the separating medium, and two identical reflecting surfaces (such that $t_1 = T_2 = T$, and $R_1 = R_2 = R$), Eq. 1.1.6 can be cast into the form

$$(1.1.7) \qquad \tau(\psi) = \tau_{max} \frac{1}{1 + H \sin^2 \psi}$$

where

$$(1.1.8) \qquad A = 1\text{-}R\text{-}T \qquad H = 4R/(1-R)^2$$

$$\tau_{max} = \left(\frac{1}{1 + A/T}\right)^2$$

$$\psi = \epsilon/2 = \varphi + \alpha/2 = \varphi + N \, k \, d \cos\theta, \quad \cos\theta = \frac{\vec{k} \cdot \vec{d}}{k \, d}$$

Fig. 1.1.2 is a plot of the Airy formula $\tau(\psi)$ vs. ψ for different values of R and for A = 0. The function peaks every time ψ is equal to an integral multiple of π. The value of the integer is the order of the interference. The distance between successive maxima is called the free spectral range since for a fixed value of d, N, and θ, this represents the change in k between adjacent orders. Notice that the maximum transmission at the center of a fringe is dependent only on the ratio A/T while the sharpness of the fringe depends only upon R.

When H is large, a single fringe is essentially Lorentzian. Let ψ be close to $m\pi$, with m an integer. Then:

$$(1.1.9) \qquad \sin^2(\psi) = \sin^2(\psi - m\pi) \simeq (\psi - m\pi)^2$$

and 1.1.7 gives:

$$(1.1.10) \qquad \frac{\tau(\psi)}{\tau_{max}} = \frac{\Gamma^2/4}{(\psi - m\pi)^2 + \Gamma^2/4}$$

where

$$(1.1.11) \qquad \Gamma = 2/\sqrt{H}$$

the full width at half maximum.

A very useful parameter is the finesse, F, defined as the ratio of the separation of successive maxima to the width Γ. Thus:

$$(1.1.12) \qquad F = \frac{\pi}{\Gamma} = \frac{\pi\sqrt{H}}{2} = \frac{\pi\sqrt{R}}{1 - R}$$

also dependent only on R.

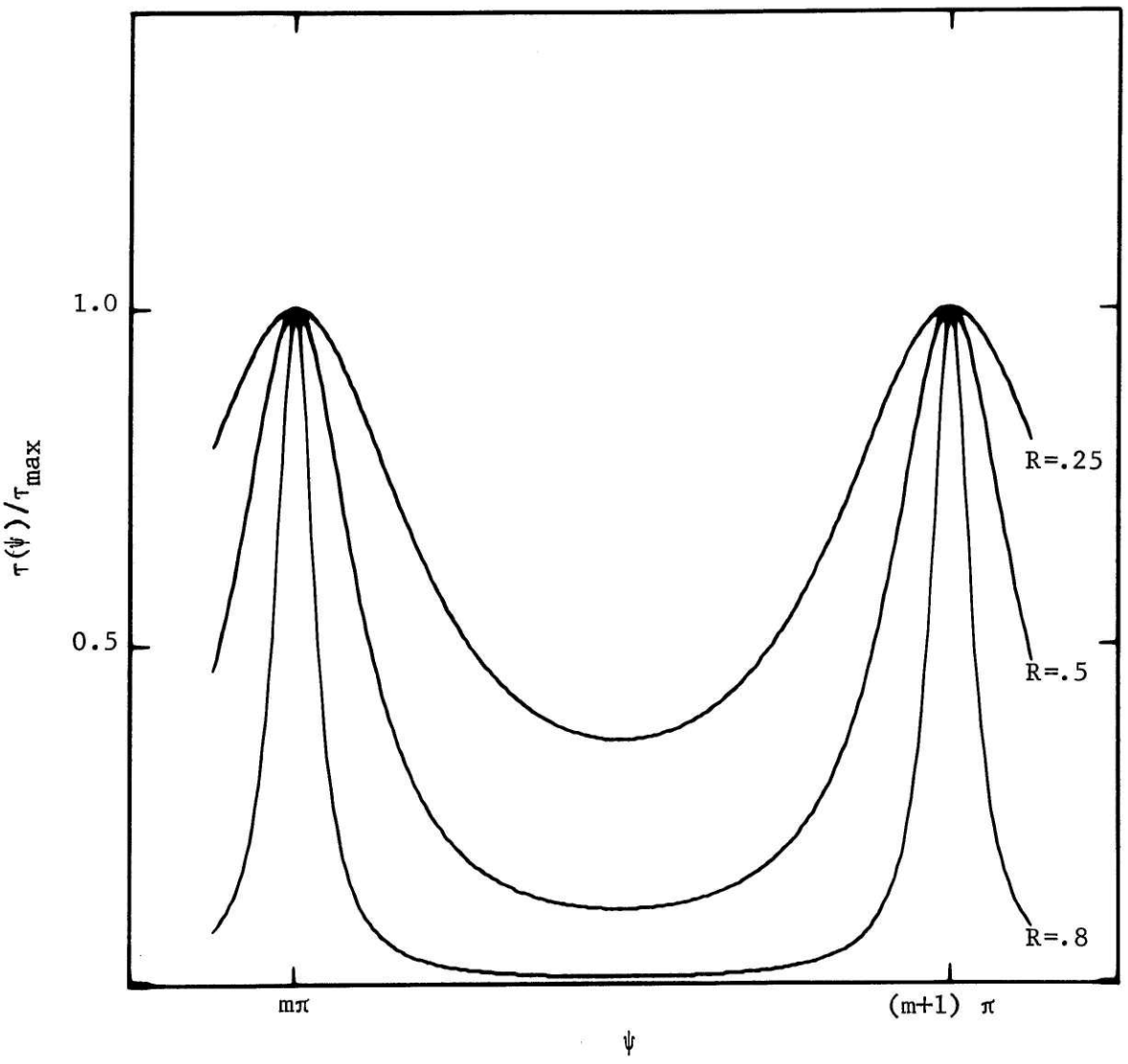

Fig. 1.1.2

SEC. 1.2 Use of the Fabry-Perot as a Spectrometer

Any Fabry-Perot interferometer is characterized by the Airy formula of Eq. 1.1.7, Fig. 1.1.2. Applications of the Fabry-Perot as a measuring instrument are based on the appearance of the several parameters in the definition, Eq. 1.1.8, of ψ. The dependence on k, d, and N is the basis of its use as a spectrometer.

The interferometer can be set to transmit a given value of k in one of three ways: By changing the spacing, d, of the surfaces, by changing the refractive index, N, of the separating medium, or by tilting the interferometer to change θ. If d is varied, care must be taken to ensure that the surfaces remain parallel, or a loss of finesse will result. Changing the index of refraction of the separating medium avoids the problems of maintaining parallelism. If the separating medium is a gas, this can be easily done by varying the gas pressure. Scanning by varying θ is almost never used since it causes a large loss of étendue, a measure of the light-gathering power of the instrument.

The resolving power, ρ, of the Fabry-Perot as a spectrometer is determined as follows: Suppose we illuminate the interferometer with radiation of two closely spaced, sharp spectral lines. We now scan the instrument by varying one of the above mentioned parameters, say d. Then a detector behind the interferometer would see the sum of two Airy functions shown in the sketch below, Fig. 1.2.1. The solid line is the Airy function for wave number k_0 and the dotted line for $k_0+\delta k$. As a criterion of ability to resolve the two lines, one can take the so-called Taylor criterion[2]

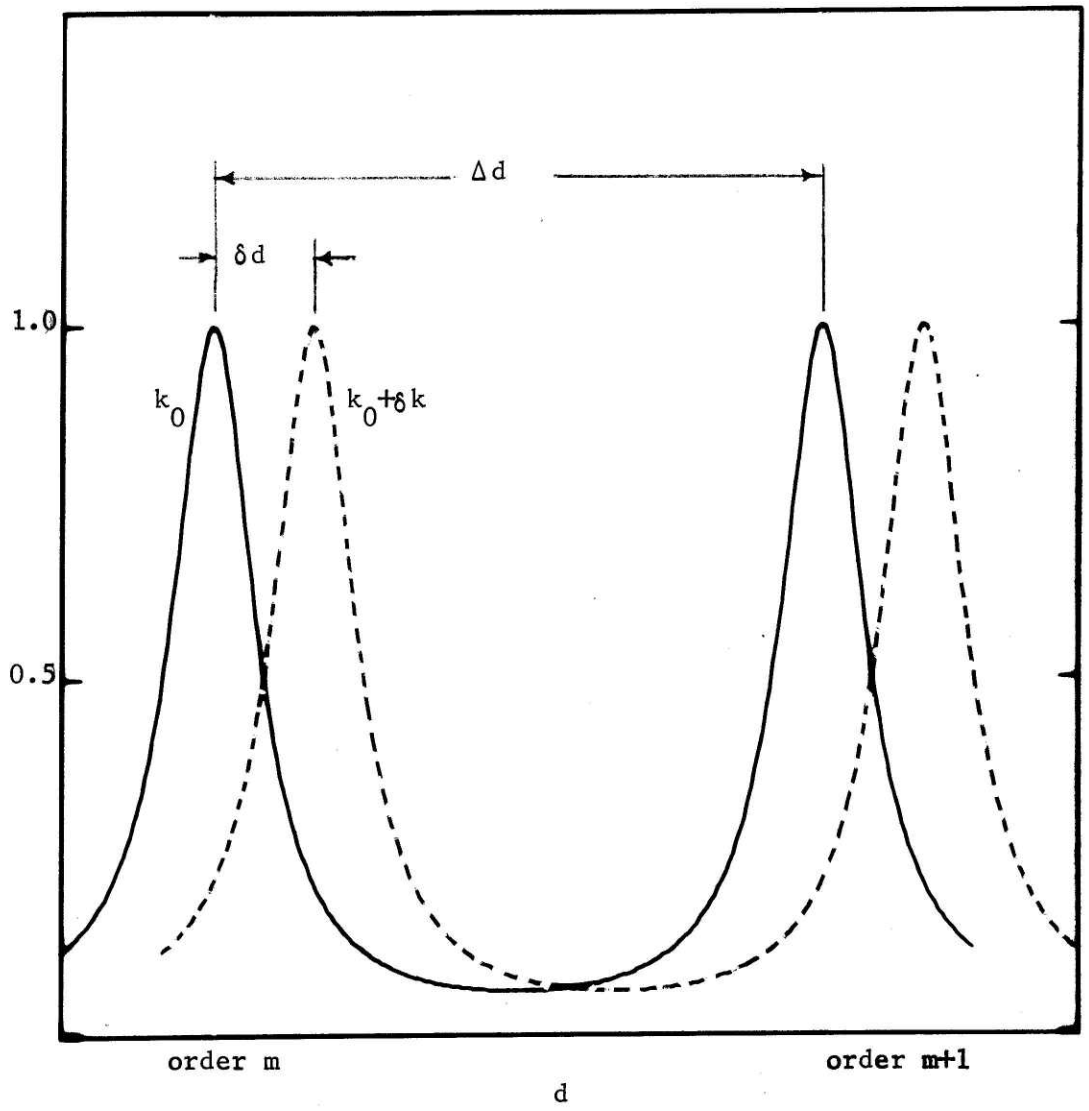

Fig. 1.2.1

(After Stone[2])

that when the two curves intersect at the half-maximum points, one can just detect that two lines are present. We assume that $\cos\theta = 1$. In addition, φ is set = 0 since we can always change d to compensate for φ. Then the maximum of order m for k_0 falls at a spacing d such that

$$(1.2.1) \qquad Nk_0 d = m\pi$$

The maximum at order m + 1 occurs for

$$(1.2.2) \qquad Nk_0(d + \Delta d) = (m+1)\pi$$

which gives

$$(1.2.3) \qquad \Delta d = \frac{\pi}{Nk_0}$$

or

$$(1.2.4) \qquad k_0 = \frac{\pi}{N\,\Delta d}$$

we can get δd by differentiating Eq. 1.2.1

$$(1.2.5) \qquad \delta d = \left| \frac{m\pi}{N} \frac{1}{k_0^2} \delta k_0 \right|$$

or

$$(1.2.6) \qquad \delta k_0 = \frac{\delta d\, N\, k_0^2}{m\pi}$$

so

$$(1.2.7) \qquad \frac{k_0}{\delta k_0} = \frac{m\,\pi\,N\,\Delta d}{\delta d\, N\, \pi} = m\,\frac{\Delta d}{\delta d}$$

but $\Delta d/\delta d$ is just the finesse of the instrument, so the resolving power,

ρ, is given by

(1.2.8) $$\rho = m F$$

As a brief illustration of its use as a spectrometer, suppose the spectrum to be studied consists of two sharp spectral lines of wave numbers k_1 and k_2; and we want to determine the difference between them. Assume the scanning method will be to vary d. We would like to operate at large order to obtain high resolution; but at the same time, we must have a free spectral range greater than $\delta k = k_2 - k_1$.

The free spectral range Δk is given by

(1.2.9) $$\Delta k = \frac{k_1}{m}$$

As long as $\delta k < \Delta k$, there will be no overlap.

We select, then, a suitable order, m, and vary d. The detector will observe peaks similar to Fig. 1.2.1, but with enough separation such that the peaks do not overlap. From Eq. 1.2.6 we have

(1.2.10) $$\delta k = \frac{\delta d\ N\ k_1^2}{m\ \pi}$$

Also we know that the first peak occurs for order m when

(1.2.11) $$k_1 = \frac{m\ \pi}{N\ d}$$

And from Eq. 1.2.4 we have

(1.2.12) $$k_1 = \frac{\pi}{N\ \Delta d}$$

Substituting the last two values of k_1 for k_1^2 in Eq. 1.2.11 we obtain

$$(1.2.13) \qquad \delta k = k_2 - k_1 = \frac{\pi}{N\,d}\,\frac{\delta d}{\Delta d}$$

It is not necessary to know d to a fraction of a wavelength or to know φ at all.

With this brief description of the Fabry-perot interferometer, we will now proceed to a description of the particular interferometer built for this thesis.

CHAPTER 2

DESIGN OF THE SCANNING FABRY-PEROT INTERFEROMETER

SEC. 2.1 Reflecting Elements

Construction of a practical far-infrared Fabry-Perot interferometer is contingent upon finding proper reflecting elements for this region of the spectrum. The necessary properties follow from the Airy formula, Eq. 1.1.7, for high maximum transmission and high finesse, $A \ll T$ and $(1-R) \ll 1$ respectively. In the far infrared, these requirements cannot be simultaneously satisfied by the usual thin homogeneous metal layers commonly used in the visible spectral region.[3] However metal grids or meshes do satisfy these requirements simultaneously, and they have previously been used with varying degrees of success.[4-12] Two dimensional mesh with square symmetry has an advantage over one dimensional grids in that the former is insensitive to the polarization of normal radiation. (This is not true, however, at other angles of incidence.) In the past decade, some types of this mesh have become commercially available; and a moderate amount of information about these meshes exists in the literature.[4-15] For these reasons, the reflecting elements of the interferometer were fabricated from metal mesh of square symmetry.

When thin two dimensional meshes first became available about ten years ago, their properties were largely unknown; and original experimenters[4-11] were forced to measure the transmission, absorption, and reflectivity of their mesh for the wavelengths of interest. Since then, some fairly good quantitative theory has been developed. Properties of the meshes have

been experimentally measured over a range of wavelengths, λ, and mesh spacings, g.[4-11] λ/g of course is the parameter responsible for the gross properties of the meshes, although the parameters a, the strip width, and t, the mesh thickness, must be included when calculating the actual values of the properties.

Ulrich[10,13] has developed a theory explaining the behavior of meshes by relating them to an electrical transmission line equivalent circuit. Building upon this and the work of others, Saksena, et. al.[14] have developed the theory we shall use here.

Saksena has determined that the intensity coefficients of reflection and transmission for the meshes should be given by:

$$(2.1.1) \qquad R = \left[1 + 4\frac{g^2}{\lambda^2}\cos^2\theta\,(F_\theta + \ln\frac{g}{2\pi a_0})^2\right]^{-1}$$

$$(2.1.2) \qquad T = 1-R = \frac{4(g^2/\lambda^2)\cos^2\theta[F_\theta + \ln(g/2\pi a_0)]^2}{1 + 4(g^2/\lambda^2)\cos^2\theta\,[F_\theta + \ln(g/2\pi a_0)]^2}$$

$$(2.1.3) \qquad F_\theta = \frac{1}{2}\sum_{n=1}^{\infty}\left\{\left[n - (1+\sin\theta)\frac{g}{\lambda}\right]^{-\frac{1}{2}}\left[n + (1-\sin\theta)\frac{g}{\lambda}\right]^{-\frac{1}{2}} + \left[n + (1+\sin\theta)\frac{g}{\lambda}\right]^{-\frac{1}{2}}\left[n - (1-\sin\theta)\frac{g}{\lambda}\right]^{-\frac{1}{2}} - \frac{2}{n}\right\}$$

$$(2.1.4) \qquad a_0 = \frac{a}{4}\left[1 + \frac{t}{\pi a}\ln(4\pi\, e\,\frac{a}{t})\right]$$

where λ, g, a, and t are as defined above, and θ is the angle of incidence. It should be pointed out that Saksena has neglected any absorptivity in deriving these formulae, but he demonstrated that this assumption was con-

sistent with his theory. We shall come back to these formulae when we calculate the theoretical finesse of the interferometer.

SEC. 2.2 Method of Scanning

As mentioned in Chpater 1, the interferometer can be scanned three different ways: by changing d, N, or θ. Because of the loss of étendue, θ-scanning was immediately rejected; leaving the other two methods, both of which have their individual disadvantages.

Since the synchrotron frequency, ω_c, in Alcator is proportional to the magnetic field strength, B, and B is inversely proportional to the major radius, R, of the machine, ω_c is also inversely proportional to R. As R changes by approximately $\pm$ 22% from the on-axis value, so ω_c will change by the same amount; and the interferometer must be capable of scanning this large range of k. To facilitate data analysis, it is desirable that this scanning range be entirely within the free spectral range of the instrument, i.e.,

$$(2.2.1) \qquad \frac{\delta k}{k} < \frac{\Delta k}{k} = \frac{1}{m}$$

or

$$(2.2.2) \qquad .22 < \frac{1}{m}, \qquad \text{or} \quad m < 4.5$$

that is, m = 4 is the largest order that can be used; and for m = 4, the scanning range needed is almost one free spectral range.

Additionally, a complete scan should only require a few milliseconds. Either one of these two requirements is sufficient to eliminate pressure scanning (changing N of the gas medium separating the meshes) as a possible method. Since N of most gases exceeds unity by only 3×10^{-4} at one atmosphere of pressure, an interferometer would have to operate with m >

3000 to be able to scan through one free spectral range with a one atmosphere change of pressure. Of course, with larger pressure changes or with gases of higher index of refraction, a lower order of interference could be used; but not as low as m = 4. In any event rapid, precise changes of pressure are difficult to make. Thus only scanning in d seemed practical.

Initial experiments involved the use of piezoelectric translators which are commonly used with visible radiation interferometers to achieve scanning times of several Hz to hundreds of kHz. However, operation in the far infrared requires three orders of magnitude more throw than operation in the visible. A piezoelectric translator with the necessary throw but designed for low frequency operation was tested. Performance was mediocre above 20 Hz; the translator could not be pushed past its design specifications.

Various mechanical schemes involving electric motors and cams were considered next, but 300 Hz is 18,000 RPM which seemed impractical to achieve without excessive vibration.

We then tried magnetic translation using a loud-speaker. Quality low frequency speakers reproduce well complex waveforms at the frequencies of interest to us, and it was thought that one might prove satisfactory for our requirements.

Accordingly we used a James B. Lansing LE-14A low frequency woofer, this particular speaker being chosen because it has a 1-1/2" diameter hole through the center of the magnet to promote better air circulation for cooling the voice coil. Only minor modifications of the original factory product were needed, namely removal of some screening at each end of the

cooling passage and the cutting of a hole in the speaker dome.

A very low-mass mesh holder was fabricated and then glued over the hole in the speaker dome. The resulting arrangement is illustrated in Fig. 2.2.1. The stationary mesh was mounted in an angular orientation mount and stacked on X-Y micrometer screw translators for final positioning and alignment. Meshes of 250 lines/inch were selected as being the most suitable of those immediately available for operation with a 337μ hydrogen cyanide laser, the radiation source used.

Let us now consider what performance is to be theoretically expected from this interferometer.

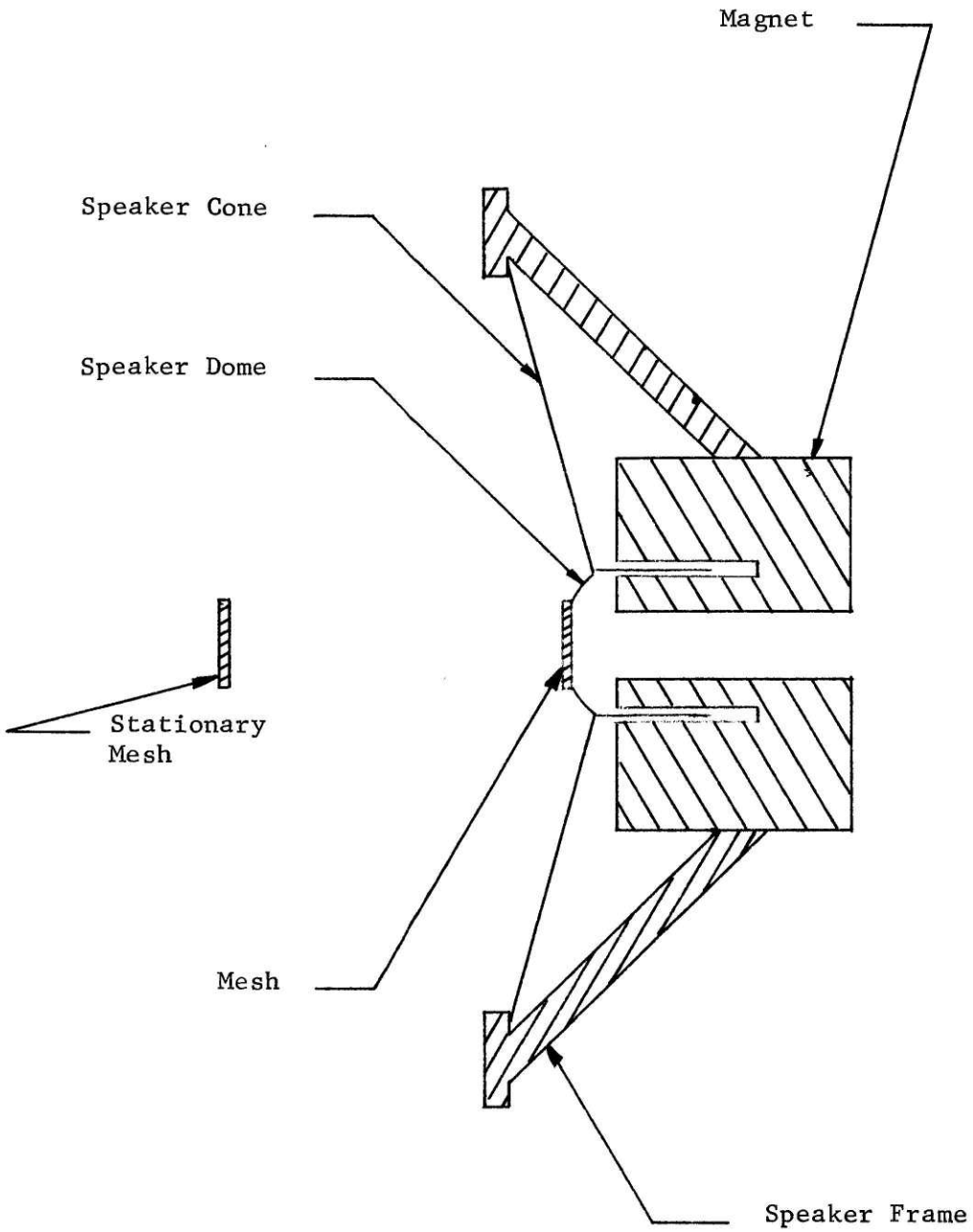

Fig. 2.2.1.

Interferometer Schematic

SEC. 2.3 Theoretical Predictions

As mentioned previously, the expected finesse is calculated from the theoretical reflectivity of the meshes given by Saksena's formulae Eqs. 2.1.1 -- 2.1.4 using the actual mesh dimensions. The 250 lines/inch mesh had $g = 102\mu$, $a = 16\mu$, and $t = 5\mu$; these parameters along with $\lambda = 337\mu$ and $\theta = 0$ give

$$(2.3.1) \qquad a_0 = 6.15\mu$$

$$F_\theta = F_0 = .053$$

and

$$R = .72$$

The theoretical finesse then is given by Eq. 1.1.10:

$$(2.3.2) \qquad F = \frac{\pi \sqrt{R}}{1-R} = 9.6$$

We then addressed ourselves to the problem of what the interferometer transmission as a function of time should be when the movable mesh was translated sinusoidally in time, a sinusoid being assumed to be the driving function the speaker could follow most accurately. Fig. 2.3.1 through Fig. 2.3.8 are plots of the function $g(x) = 1 / (1 + H \sin^2(B \sin x))$ vs. x for various values of B with H derived from the theoretical finesse. They therefore predict what the interferometer transmission should look like when the speaker is driven with a voltage given by $V = V_0 \sin \omega t$ as V_0 is increased.

Figs. 2.3.7 and 2.3.8 are especially interesting since the sharp peaks in the center occur when the velocity of the moving mesh is essentially

constant. As such they are a direct indication of the finesse. This will be the experimental basis to determine the finesse when the mesh is moving to verify that the finesse does not change from its stationary ("D.C.") value.

B = .67

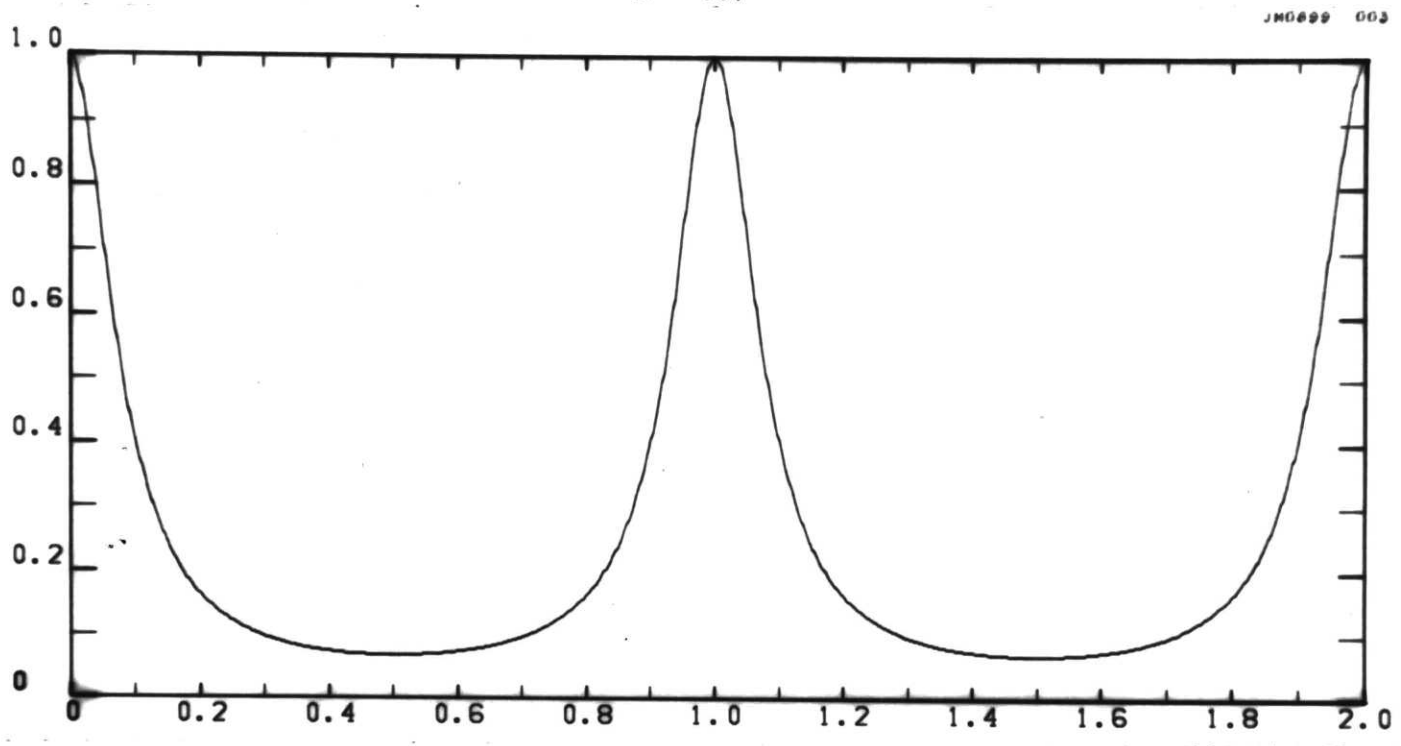

Fig. 2.3.1

B = 2

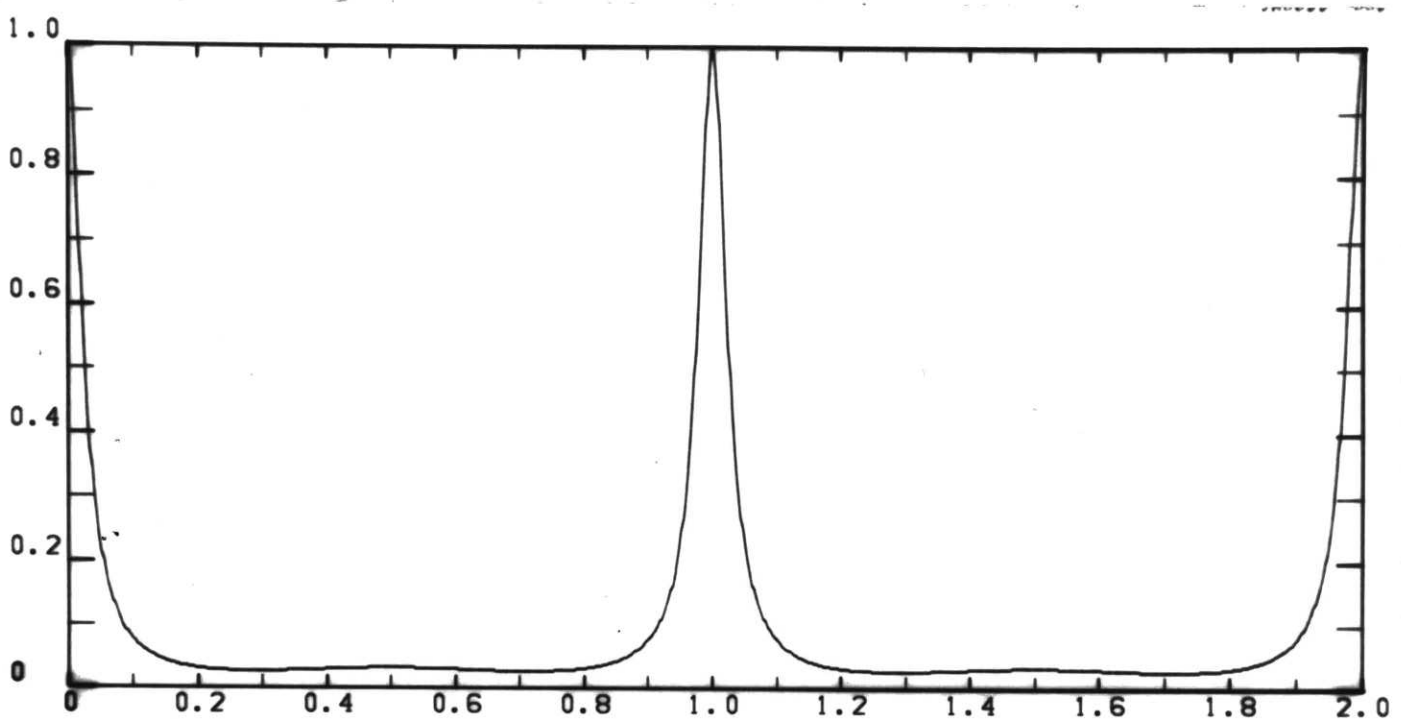

Fig. 2.3.2

B = 3

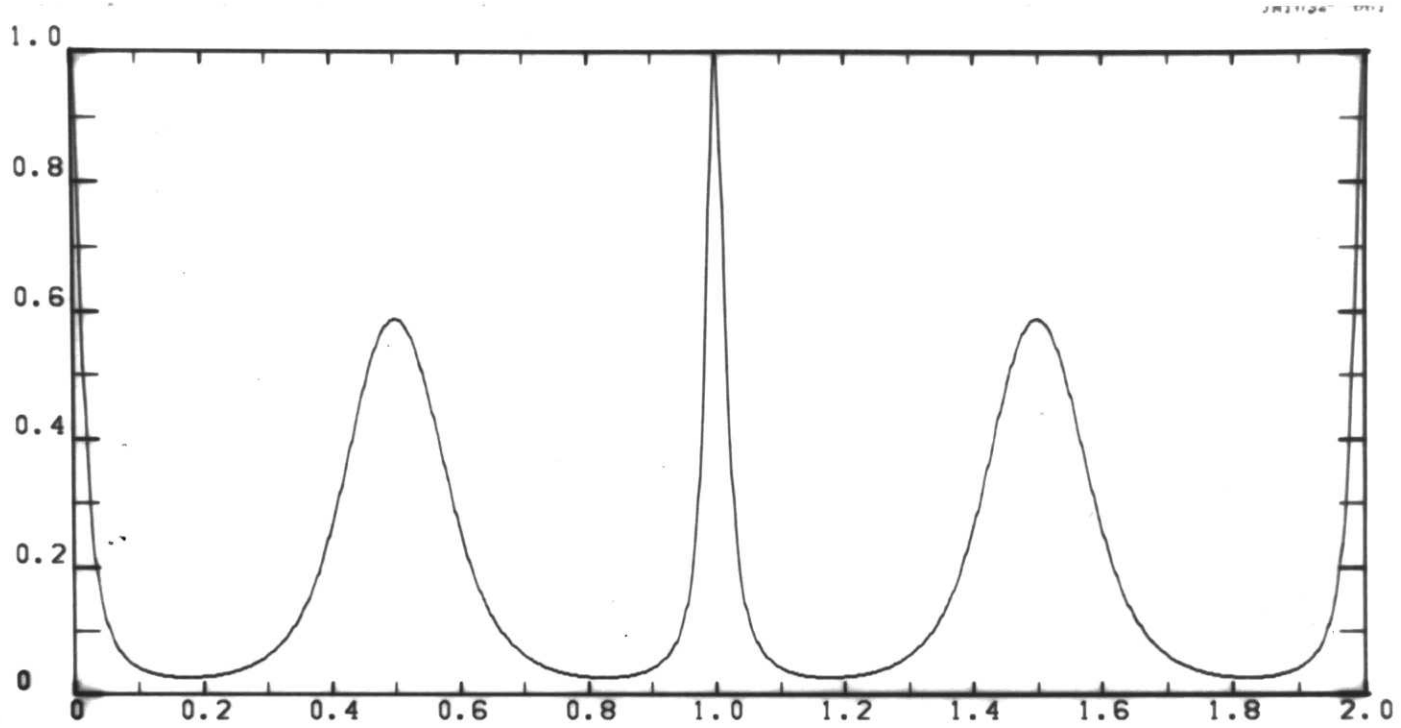

Fig. 2.3.3

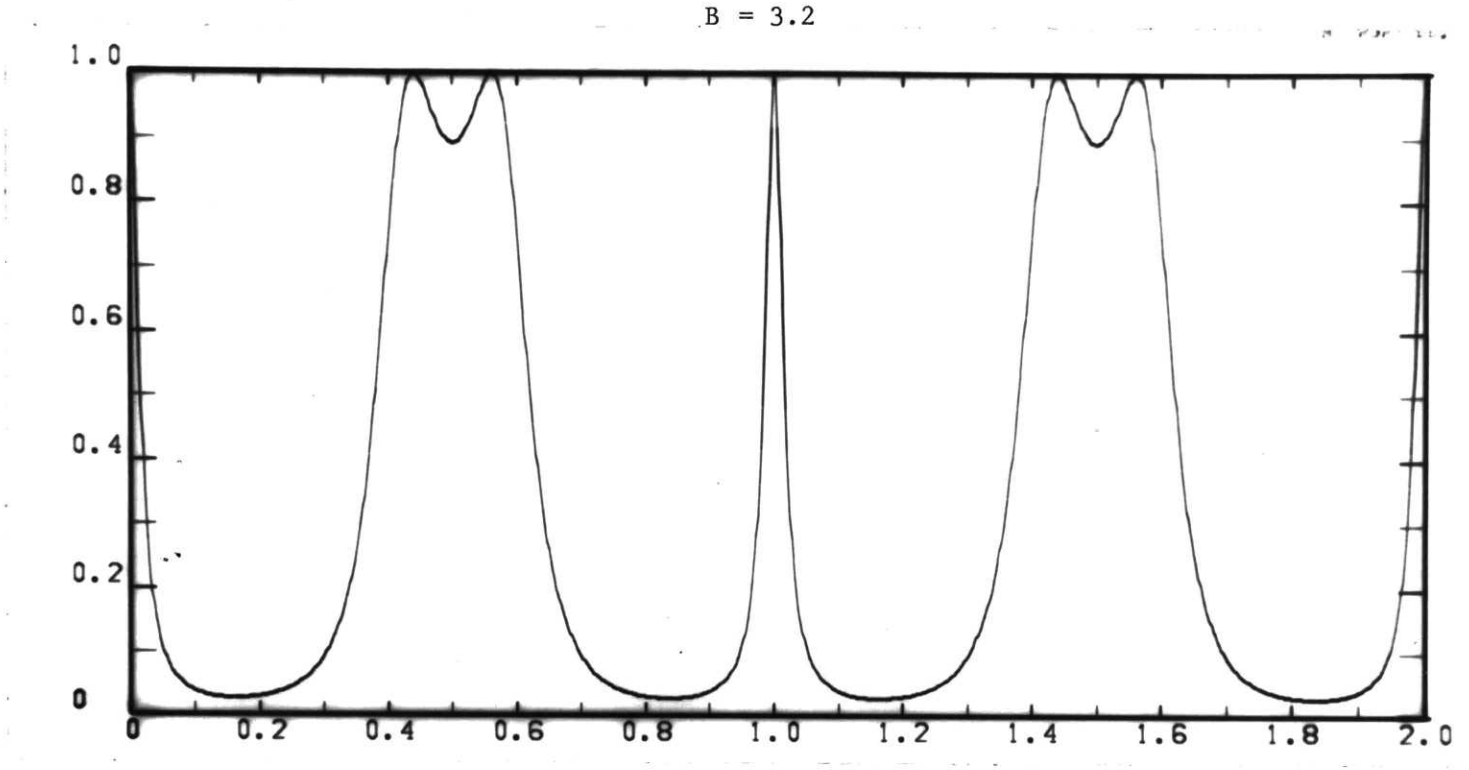

Fig. 2.3.4

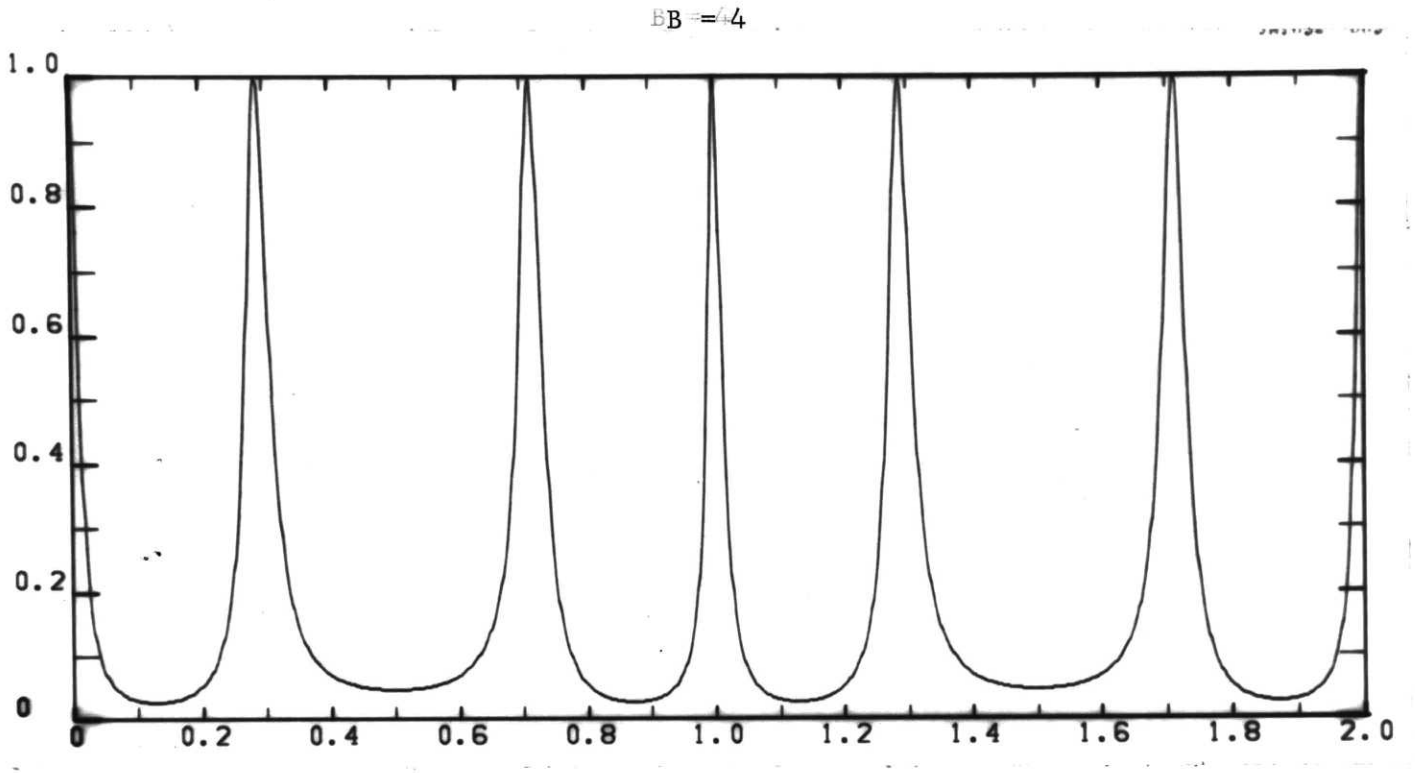

Fig. 2.3.5

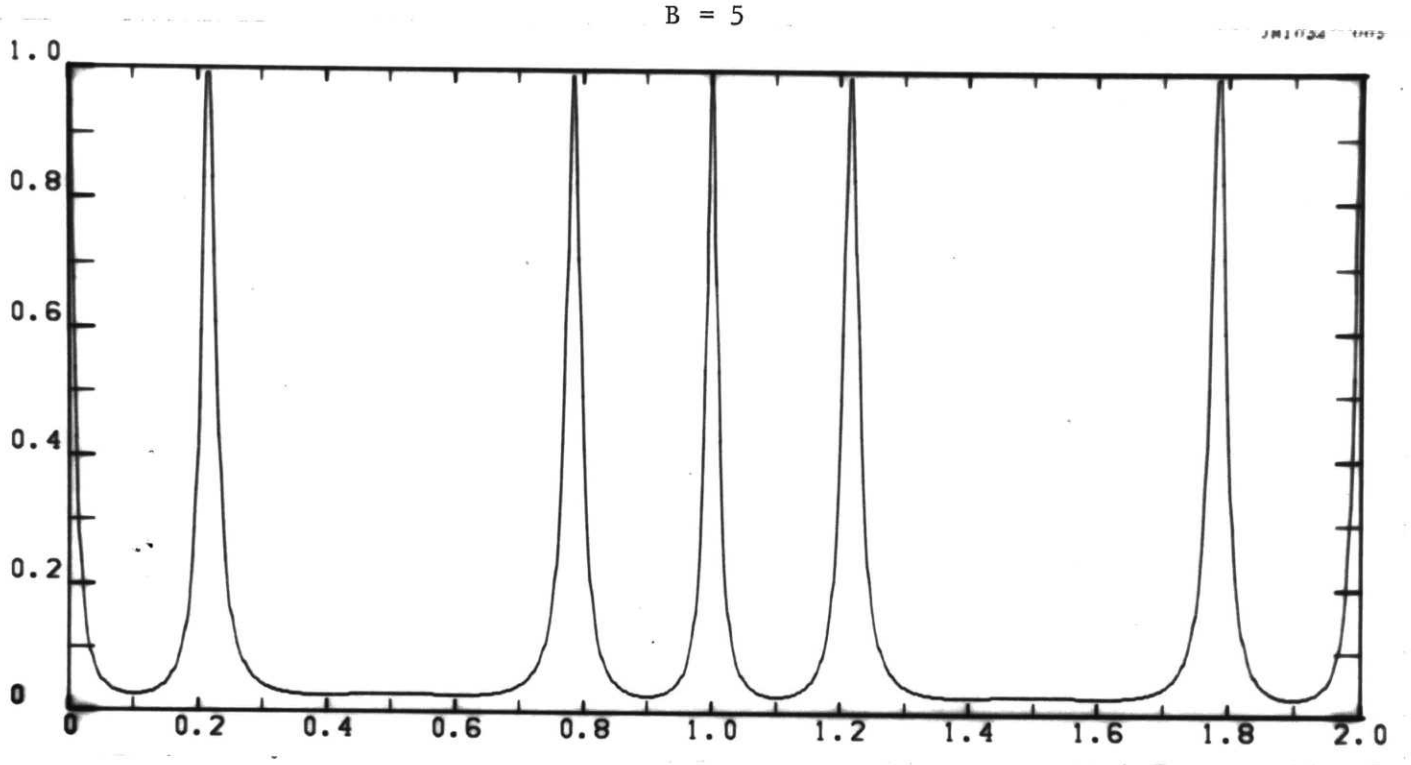

Fig. 2.3.6

B = 6

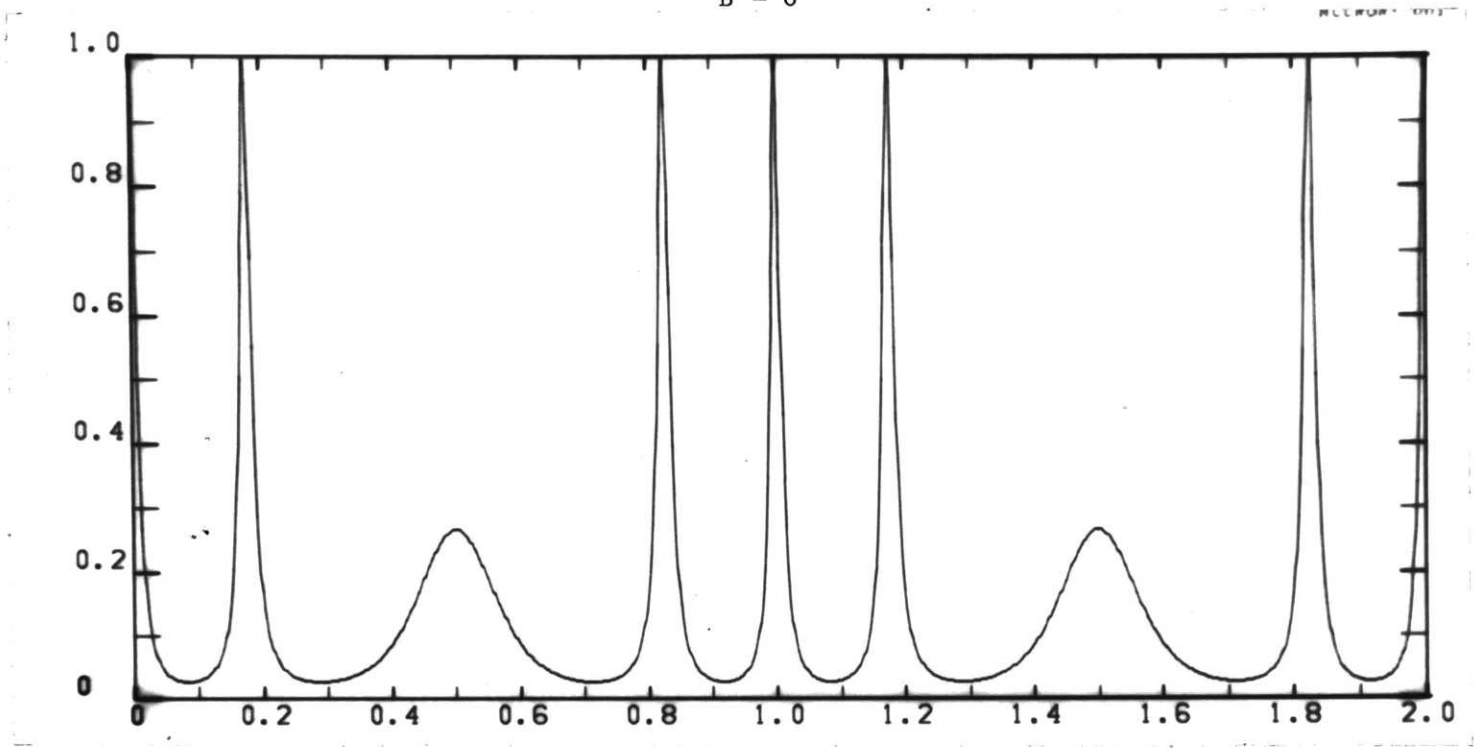

Fig. 2.3.7

B = 6.34

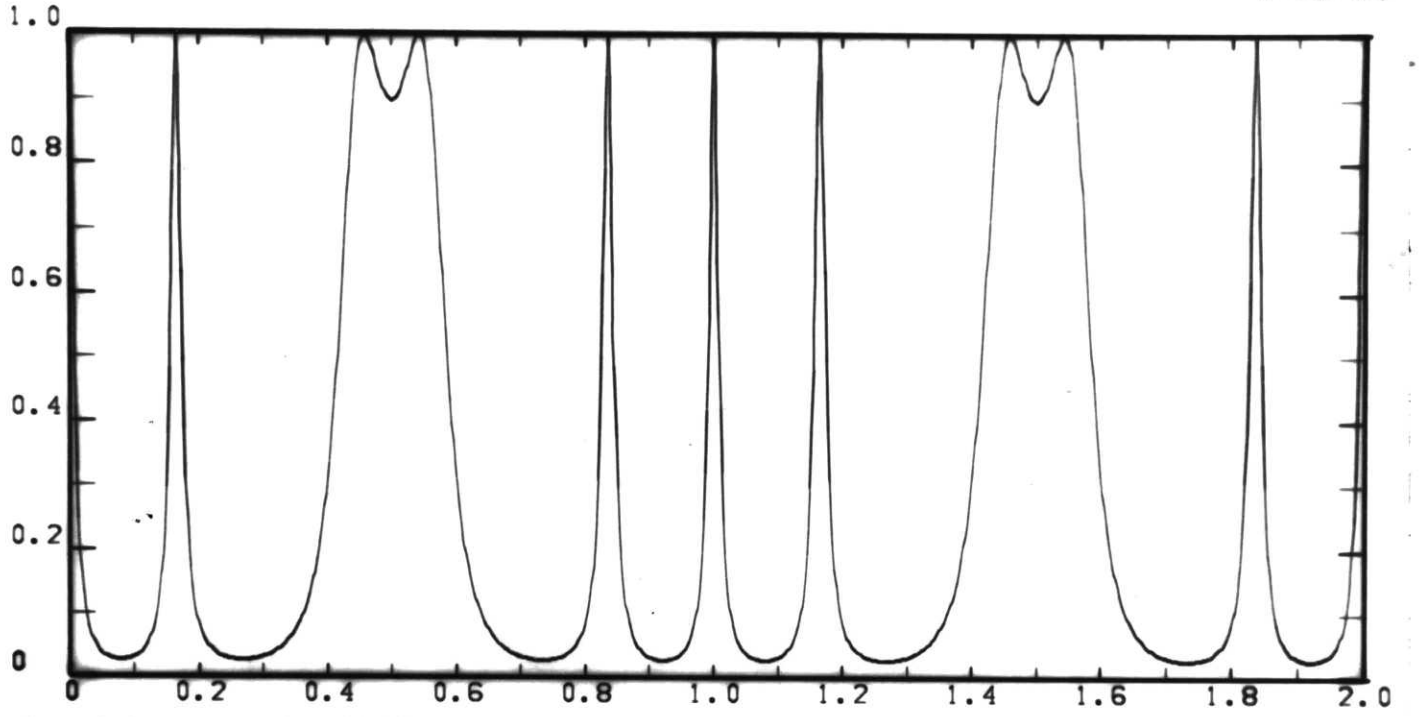

Fig. 2.3.8

CHAPTER 3

EXPERIMENTAL RESULTS

SEC. 3.1 Experimental Set-Up

Testing of the interferometer was done at λ = 337 with the radiation from a HCN laser. The radiation transmitted through the interferometer was condensed with a hollow copper cone onto a 2 mm $\times$ 2 mm monocrystalline triglycine sulfate (TGS) pyroelectric detector, described elsewhere.[16] As these detectors are somewhat noisy, a lock-in amplifier and mechanical chopper were used to improve the signal-to-noise ratio.

The frequency response of the detector was measured and found to be flat from 40 Hz to above 1 kHz. Below 40 Hz, the detector was limited by the coupling capacitors in the following preamp; and above 1 kHz, the detector response falls off as 1/f due to the internal capacitance of the TGS crystal. Unfortunately we do not accurately know where the 1/f region began. These frequency response measurements were made with a mechanical chopper that could not be driven any faster than 750 cycles/sec. We only know that the 1/f break-point was somewhere between 1 kHz and 5 kHz. Fortunately, this did not have any serious effect on the experiment.

SEC. 3.2 D.C. Response

The D.C. (no magnetic translation) response of the interferometer was measured by scanning in d with the micrometer screw on the X translator. Figs. 3.2.1 -- 3.2.5 show the response at various mesh spacings, d. The X-axis positions are merely the relative position indicated by the micrometer. The Y-axis scale is completely arbitrary, but in each case the peak transmission was 0.66 absolute.

The observed points, indicated by circles in the figures, were fitted with a least-squares fit by the function

$$(3.2.1) \qquad y(x) = \frac{C}{1 + H \sin^2(\varphi + Bx)}$$

where C, H, φ and B are constants, whose values are determined by the solution of the least-squares' normal equations by way of the Leveberg-Marquardt algorithm.[17-20] The solid line is the fitted function, and the indicated finesse was derived from the least-squares value of H.

The five values give a measured finesse of F = 9.3 $\pm$.2 which corresponds to a mesh reflectivity of 0.71, good agreement with the result predicted from Saksena's formulae. Since the peak transmission was 0.66, T = .24 and A = .05, a value for the absorption considerably larger than that predicted by Saksena. This value of absorptivity does, however, agree well with that measured by Vogel and Genzel[7] and Mitsuishi, et. al.[5] We conclude that the D.C. response is essentially that predicted by theory.

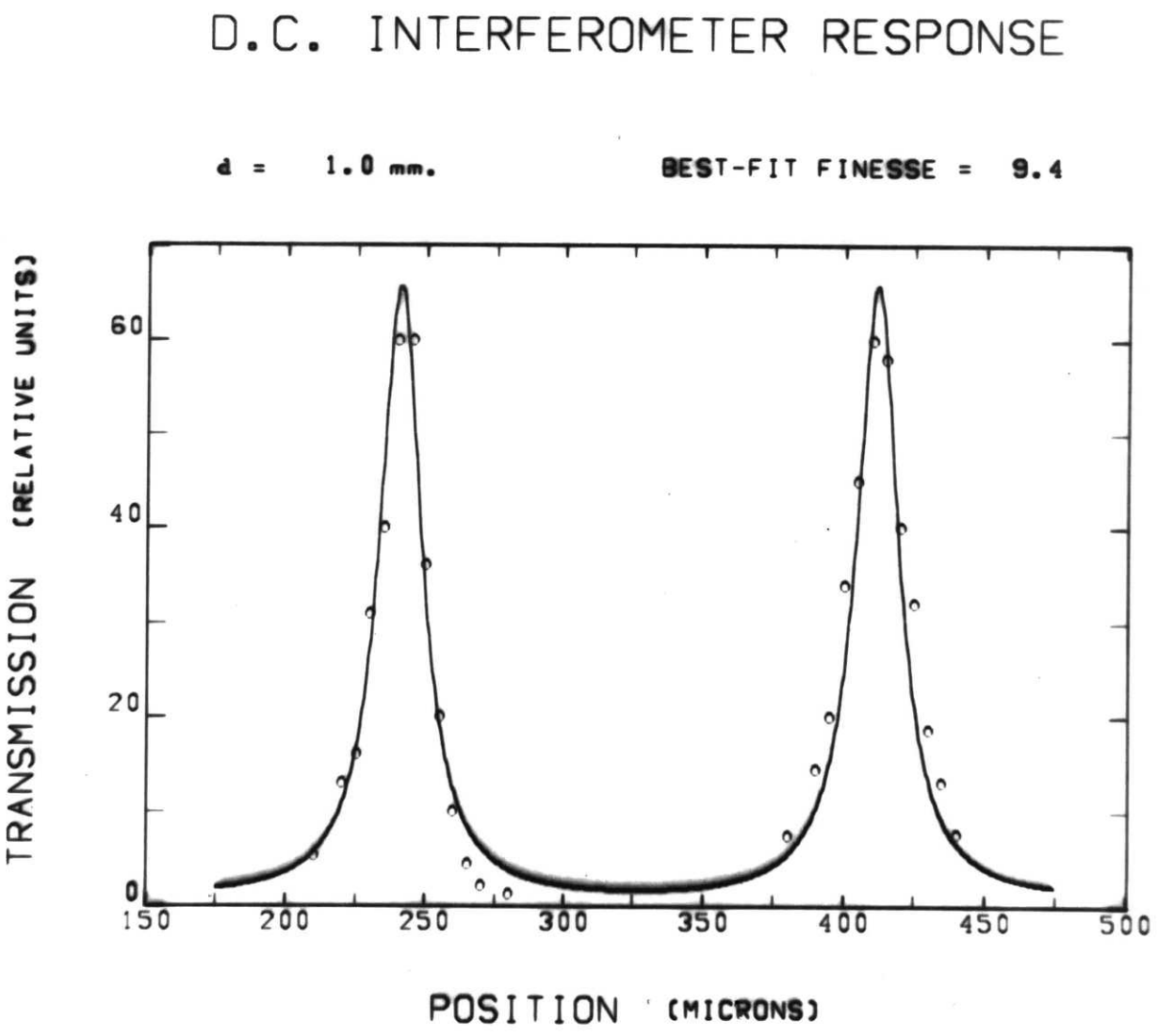
D.C. INTERFEROMETER RESPONSE
d = 1.0 mm.
BEST-FIT FINESSE = 9.4
TRANSMISSION (RELATIVE UNITS)
0
20
40
60
150
200
250
300
350
400
450
500
POSITION (MICRONS)

Fig. 3.2.1

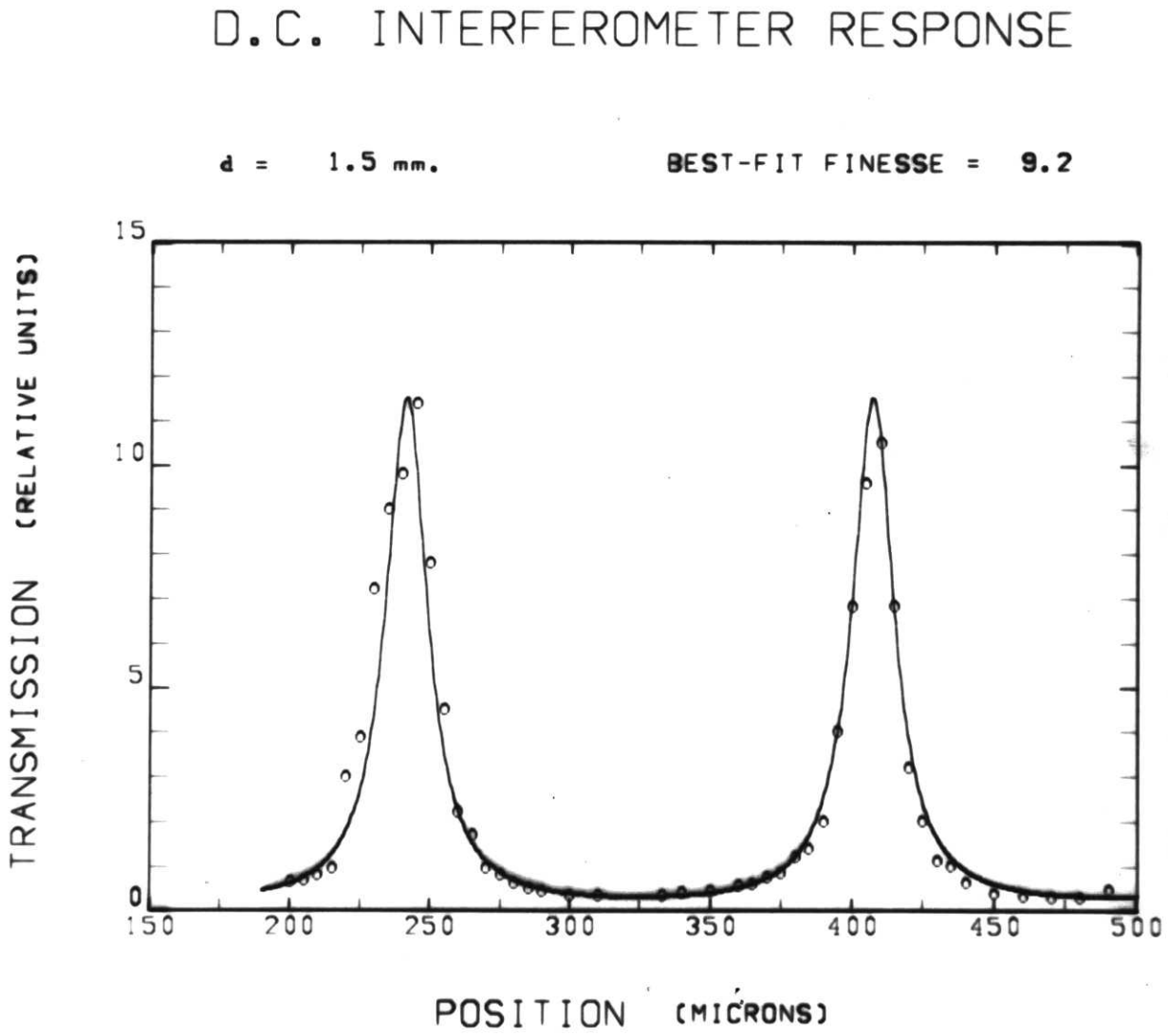
D.C. INTERFEROMETER RESPONSE
d = 1.5 mm.
BEST-FIT FINESSE = 9.2
TRANSMISSION (RELATIVE UNITS)
15
10
5
0
150
200
250
300
350
400
450
500
POSITION (MICRONS)

Fig. 3.2.2

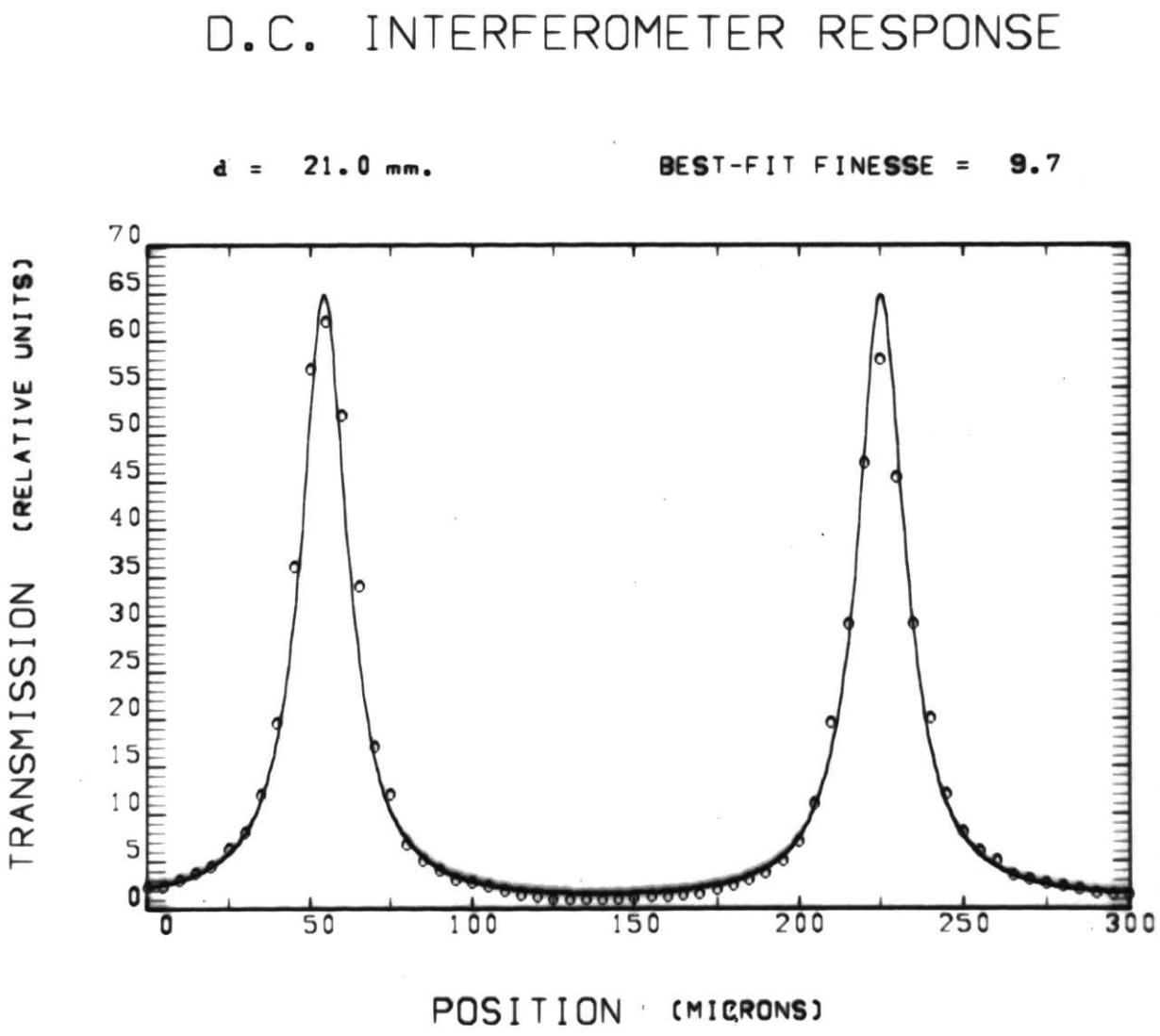
D.C. INTERFEROMETER RESPONSE
d = 21.0 mm.
BEST-FIT FINESSE = 9.7
TRANSMISSION (RELATIVE UNITS)
0
5
10
15
20
25
30
35
40
45
50
55
60
65
70
0
50
100
150
200
250
300
POSITION (MICRONS)

Fig. 3.2.3

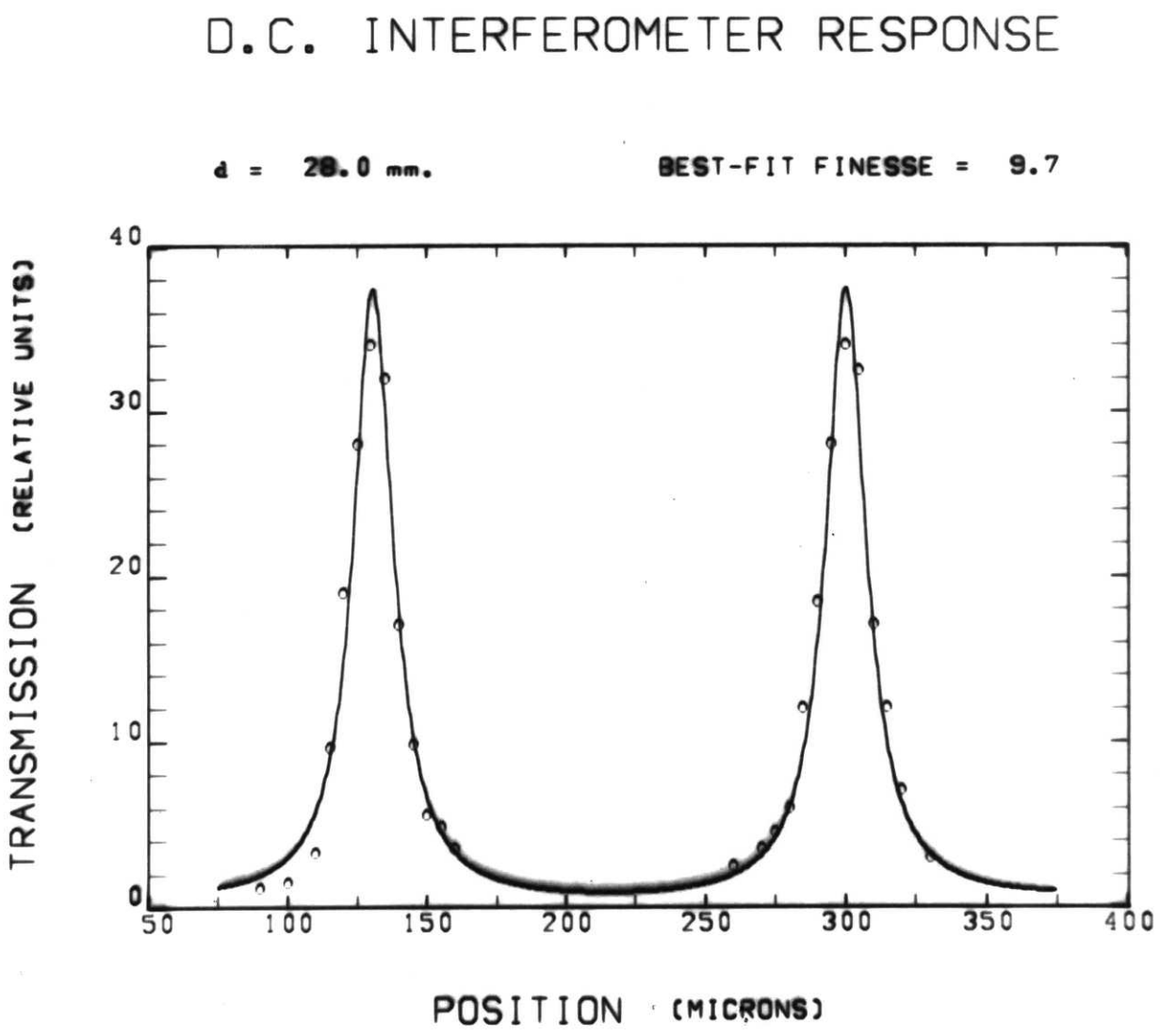
D.C. INTERFEROMETER RESPONSE
d = 28.0 mm.
BEST-FIT FINESSE = 9.7
TRANSMISSION (RELATIVE UNITS)
0
10
20
30
40
50
100
150
200
250
300
350
400
POSITION (MICRONS)

Fig. 3.2.4

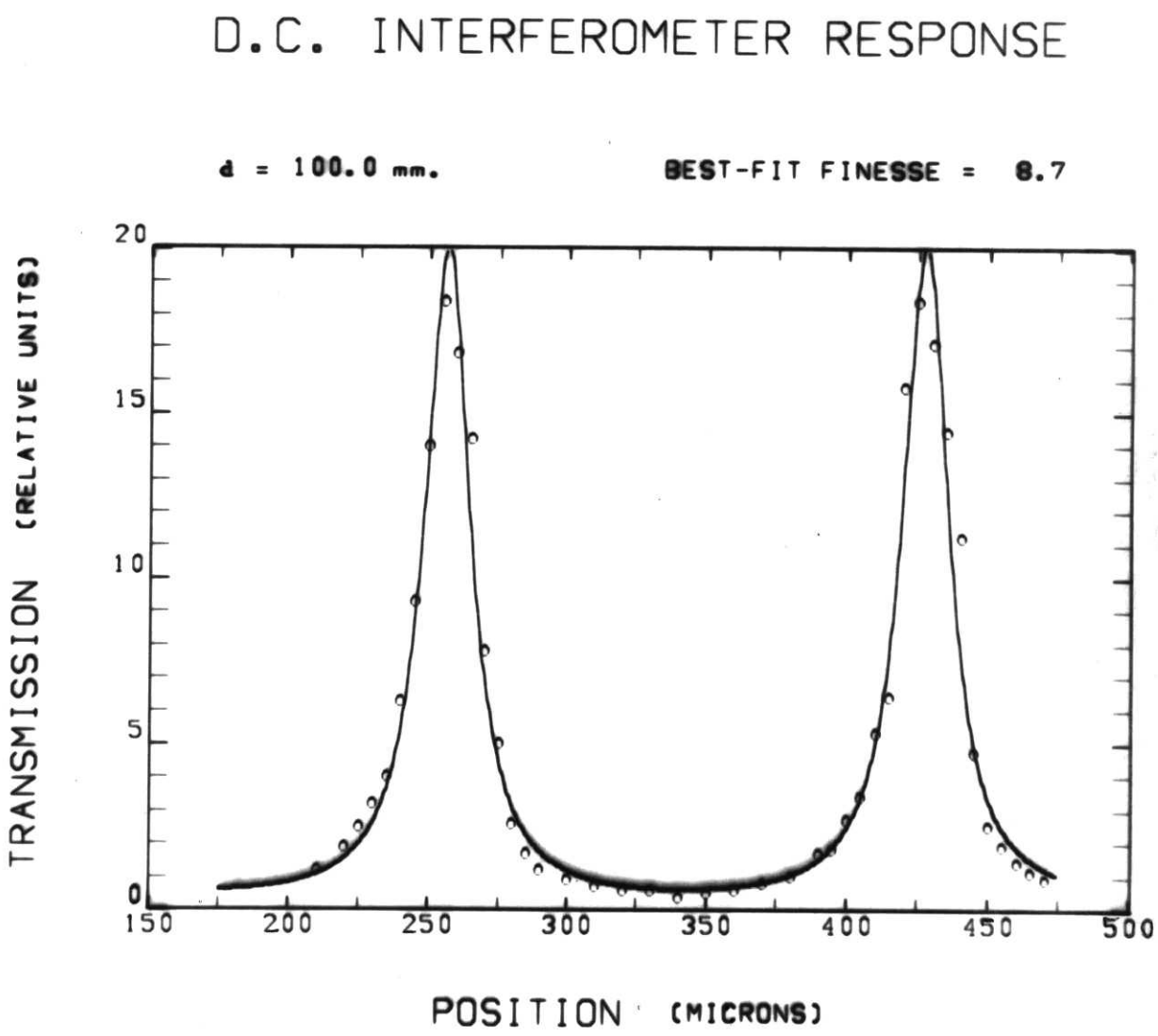
D.C. INTERFEROMETER RESPONSE
d = 100.0 mm.
BEST-FIT FINESSE = 8.7
TRANSMISSION (RELATIVE UNITS)
20
15
10
5
0
150
200
250
300
350
400
450
500
POSITION (MICRONS)

Fig. 3.2.5

SEC. 3.3 A.C. Response

During the A.C. response measurements, the speaker was driven sinusoidally, $V = V_0 \sin(2\pi\nu t)$, at different frequencies, ν, and voltages, V_0. The output from the detector was put on the vertical axis of an oscilloscope and the time-base adjusted so that the sweep took one period of the sinusoid. Figs. 3.3.1 -- 3.3.4 are pictures of the trace for ν = 50 Hz as the voltage V_0 was increased for a mesh separation of d = 1 mm. It was readily apparent that the transmission was as expected. Driving frequencies of ν = 30, 50, and 80 Hz were applied; and in every case, the results were exactly as those of Figs. 3.3.1 -- 3.3.4.

The analysis of these results is facilitated by reference to Fig. 2.3.8; the same comments apply to the bottom picture of Fig. 3.3.4. The peak at X = 0 corresponds to the mesh in its center position, Z = 0, when V = 0. The peak at X = .17 occured when the mesh had moved to $Z = \lambda/2$ in the positive direction, the peak at X = .46 when the mesh had been displaced to $Z = \lambda$, and the dip at X = .5 marked the maximum excursion of the mesh in positive direction when $V = V_0$. At this point the mesh retracted, moving back through the two transmission peaks to Z = 0 at X = 1 in Fig. 2.3.8. As the sinusoid then went negative, the whole process repeated, but in the negative direction. Every $\lambda/2$ of displacement was a scan of one free spectral range. Thus in one period of the applied sinusoid, we had eight complete scans of the interferometer, for an effective scanning frequency of 400 Hz.

The analysis of other values of V_0 is similar.

The 1/f falloff in detector response can be seen in the bottom photo-

graph of Fig. 3.3.4. Note that the sharp fringes, corresponding to the highest mesh velocity, were clearly reduced in amplitude from the peaks occuring when the mesh was moving slowly. A single sharp fringe had a characteristic time of less than one millisecond putting it into the 1/f region of the detector. Since the A.C. finesse was to be determined from these sharp fringes, as mentioned in Sec. 2.3, we had to determine what, if any, effect this 1/f falloff would have on the measured finesse.

After some momentary reflection, we realized that the falloff could only reduce the measured finesse from its actual value. This can be easily seen by treating a fringe as a single input pulse falling on the detector. Then the output pulse from the detector is the convolution of the input pulse with the response function of the detector. We recall from the theory of Fourier transforms that the convolution is the inverse Fourier transform of the product of the two Fourier transforms of the input pulse and the detector response.[21] The transform of the detector response we know: It is equal to one out to some cutoff frequency $\nu_c \approx 1.5$ kHz and then falls off as $1/\nu$. We do not know the transform of the input pulse. We do know, however, as a general property of Fourier transforms, that the sharper the input pulse is in time, the broader its transform is in ν.[22] Due to the shape of the transform of the detector response, the product of the two transforms can never be broader than the transform of the input pulse; it can only be narrower.

Since the product can only be narrower than the input pulse transform, it follows immediately that the convolution, the inverse Fourier transform, can only be broader than the input pulse. Hence the measured finesse can

only be lower than the true value.

The finesse was measured at each frequency by increasing V_0 to give a display of the type of the bottom photograph of Fig. 3.3.4. The trace was then magnified five times, and the central three fringes photographed. Fig. 3.3.5 is an example for ν = 50 Hz with the magnified image below. Fig. 3.3.6 are the traces for ν = 30 Hz and 80 Hz. In the 80 Hz case notice the slow falloff of the peaks due to the pyroelectric crystal thermal junction anomalies.[23] This effect is also noticable in the 50 Hz case, but to a lesser extent.

The finesse was determined from measurements off the film of the ratio of the inter-order spacing to the fringe width. In the case of 50 Hz and 80 Hz, a perpendicular was dropped from the top of the fringe, and the half width to the leading edge measured. The finesses and their uncertainties due to difficulties of measuring off the films were $9.0 \pm .3$, $9.5 \pm .8$, and 9 ± 1 for 30 Hz, 50 Hz, and 80 Hz, respectively. Any degradation of the measured finesse due to 1/f falloff was apparently masked by the uncertainties of measurement. In any event, we conclude that the A.C. finesse is at least 90% of the D.C. value.

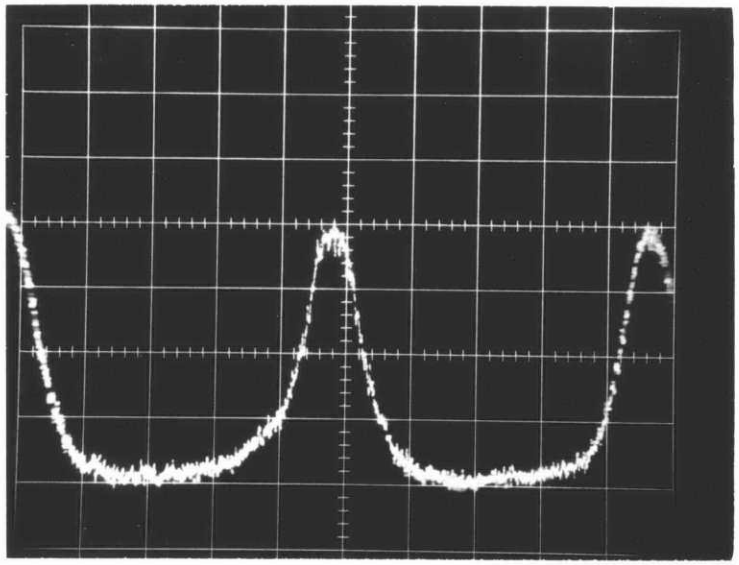

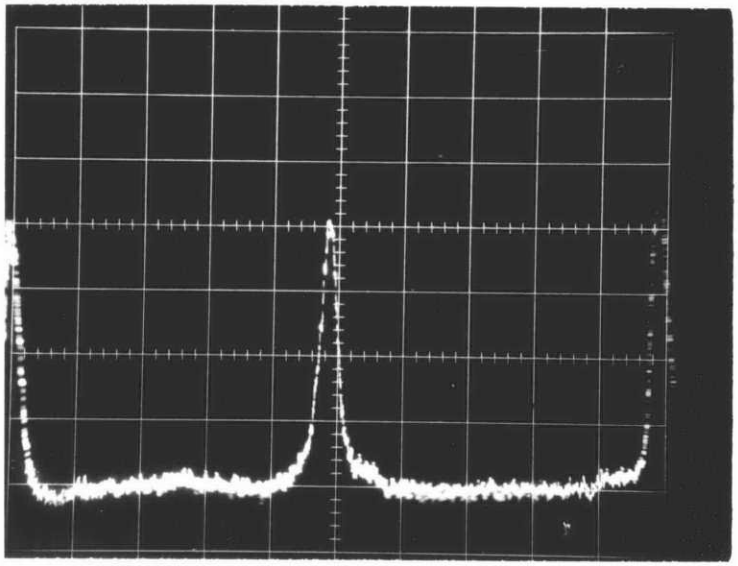

Fig. 3.3.1

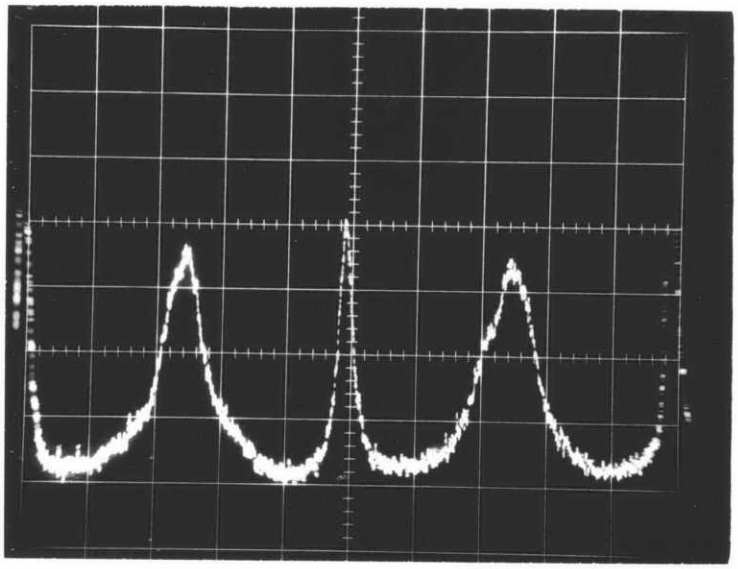

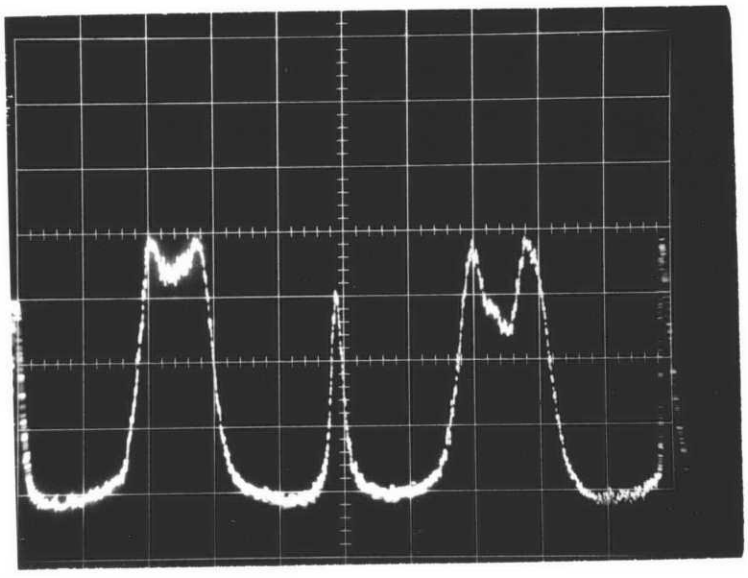

Fig. 3.3.2

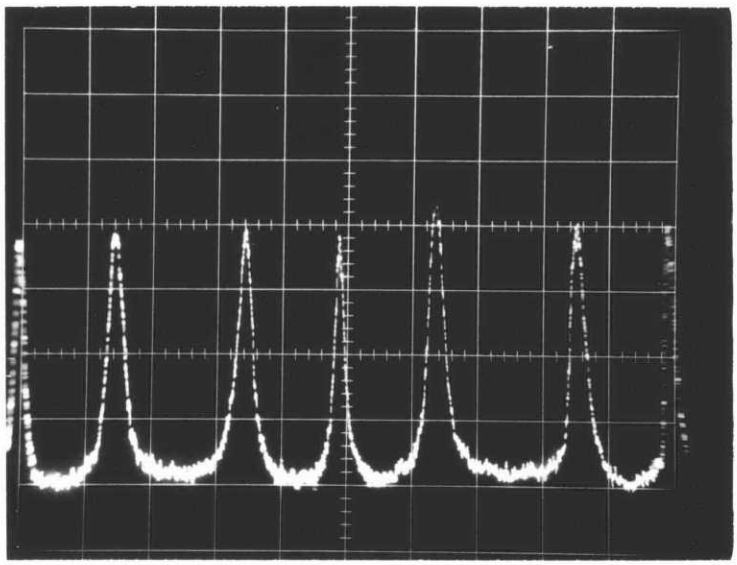

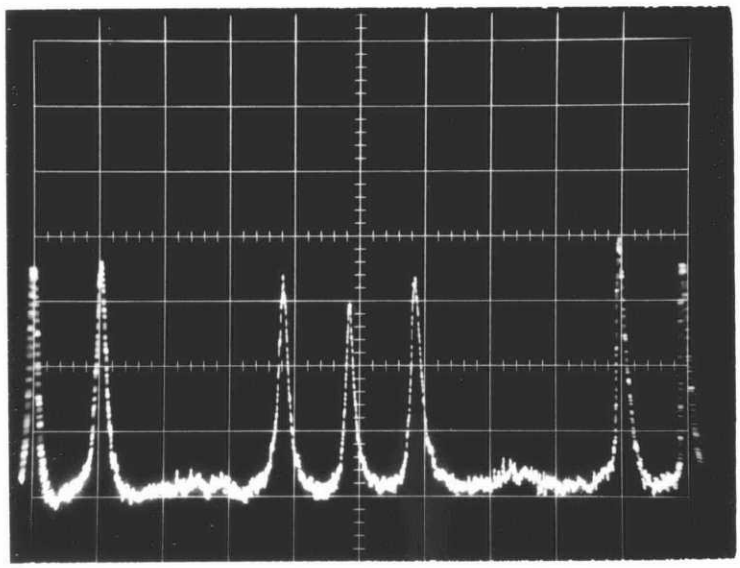

Fig. 3.3.3

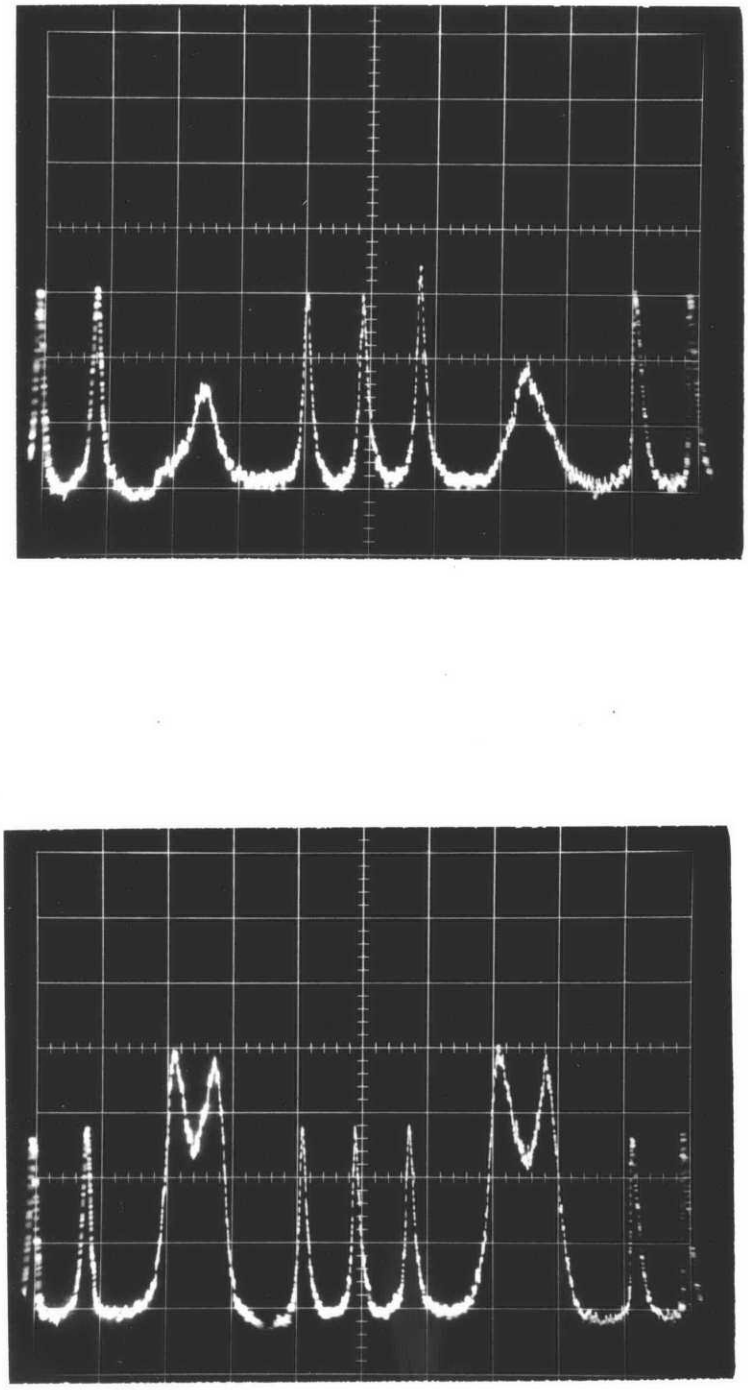

Fig. 3.3.4

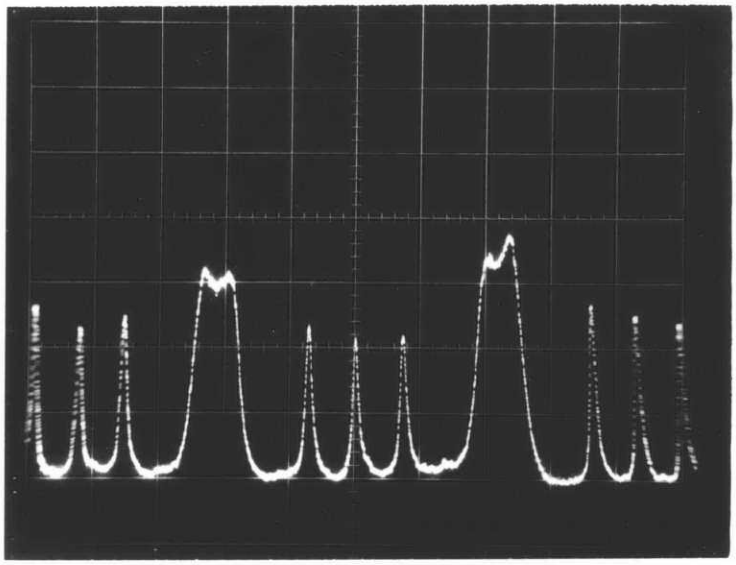

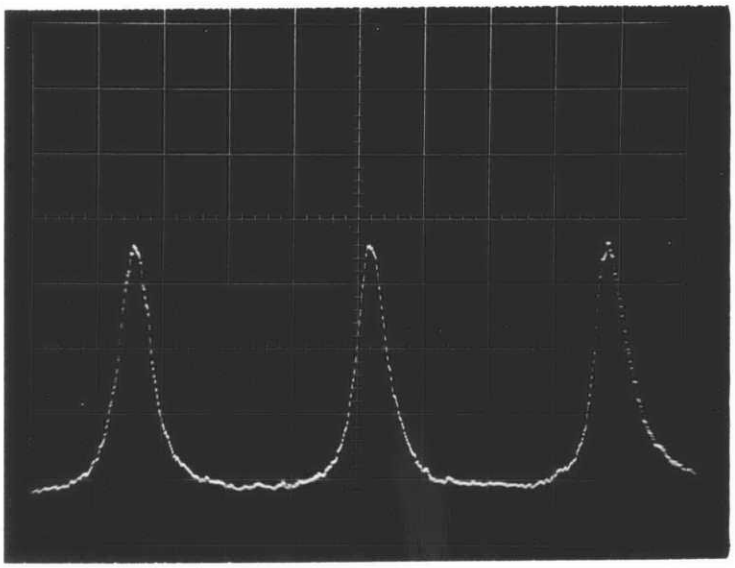

Fig. 3.3.5

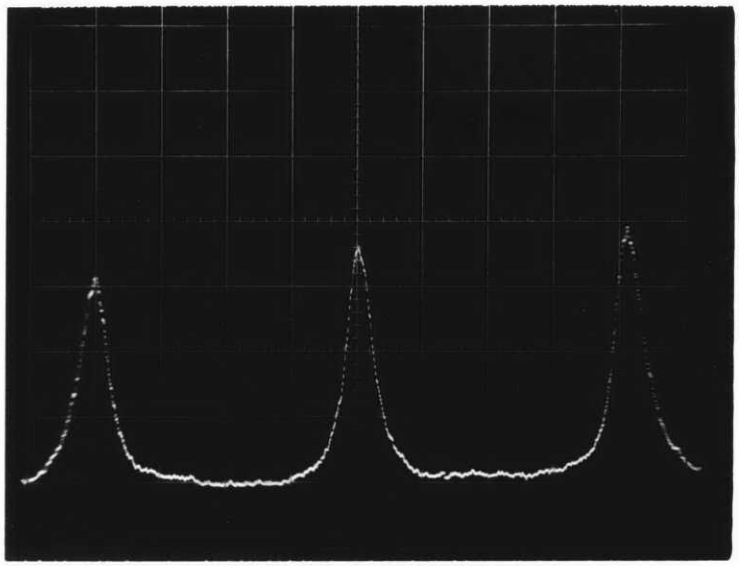

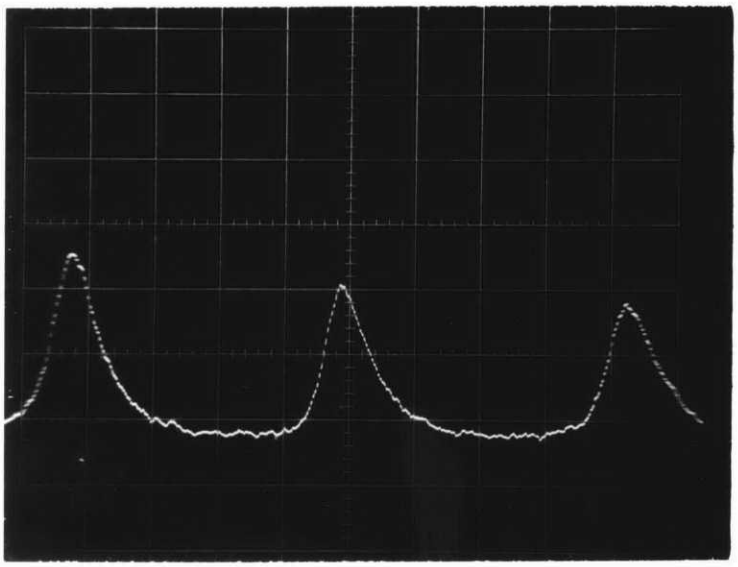

Fig. 3.3.6

CONCLUSION

There can be no doubt that the concept of magnetic translation works, and works well. This fast-scanning Fabry-Perot is easy to construct and virtually fool-proof. To obtain a given finesse at a specified wavelength, it is only necessary to select the proper mesh. Since meshes with 1000 lines/inch are available, this interferometer should be usable with a finesse of 10 at wavelengths down to at least 100μ. Conversely meshes are available with as few as 30 lines/inch so the interferometer should be usable at 5 mm or longer wavelengths. There are, however, several factors limiting how far the usable spectral range can be extended.

At short wavelengths, the alignment and uniformity of the mesh spacing becomes increasingly critical. For a given finesse and wavelength, the mesh spacing must be uniform within $d = \lambda/(2F)$.[6] For a finesse of 10 at $\lambda = 100\mu$, this means $d = 5\mu$. For the same reason parallelism must be maintained within several seconds of arc. As the mesh is translated through greater and greater distances, some wobble in the speaker cone is inevitable, and this will certainly limit the maximum scanning frequency.

Conversly at longer wavelengths, alignment becomes less critical. However the size of the hole in the magnet structure will be a limiting factor due to diffraction effects. Increasing the hole diameter, of course, removes this restriction. For microwave applications, the magnet structure would have to be specially fabricated as a separate unit with as large a bore as necessary.

In any event, the interferometer we have constructed is usable over an

order of magnitude range of wavelengths with a scanning time of three milliseconds or less.

REFERENCES

[1]Steel, W.H.; Interferometry; (Cambridge: Cambridge University Press, 1967) pp. 109 - 131.

[2]Stone, J.M.; Radiation and Optics; (New York: McGraw-Hill Book Co., 1963) pp. 409 ff.

[3]Hadley, L.N. and Dennison, D.M.; J. Opt. Soc. Amer., 37, 451 (1947).

[4]Renk, K.F. and Genzel, L.; App. Opt., 5, 643 (1962).

[5]Mitsuishi, A. et. al.; Jap. J. App. Phys., 2, (1963).

[6]Ulrich, R. et. al.; IEEE MTT, 11, 363 (1963).

[7]Vogel, P. and Genzel, L; IR Phys., 4, 257 (1964).

[8]Vinogradov, E.A. et. al.; JETP Lett., 2, 205 (1965).

[9]Balakhanov, V.Ya. et. al.; Sov. Phys. Tech. Phys., 11, 1032 (1967).

[10]Ulrich, R.; IR Phys., 7, 37 (1967).

[11]Rawcliffe, R.D. and Randall, C.M.; App. Opt., 6, 1353 (1967).

[12]Ulrich, R.; App. Opt., 7, 1987 (1968).

[13]Ulrich, R.; IR Phys., 7, 65 (1967).

[14]Saksena, B.D. et. al.; IR Phys., 9, 43 (1969).

[15]Pradhan, M.M.; IR Phys., 11, 241 (1971).

[16]Barnes Engineering Co.; "Application Notes for Pyroelectric Detectors", Bul. #2-611; 30 Commerce Rd., Stamford, Conn.

[17]MIT Information Processing Center; Pub. #AP-84 (1972).

[18]Levenberg, K.; Quar. App. Math., 2, 164 (1944).

[19]Marquardt, D.W.; J. Soc. Indust. App. Math., 11, 431 (1963).

[20]Bevington, P.R.; Data Reduction and Error Analysis in the Physical Sciences; (New York: McGraw-Hill Book Co., 1969).

[21]Sneddon, I.H.; The Use of Integral Transforms; (New York: McGraw-Hill Book Co., 1972) p.60.

[22]Ibid; p. 52.

[23]See reference #16 for a discussion of the interaction of capacitive and thermal effects in pyroelectric crystals.